ARTICLES
PUBLISHED ONLINE: 11 SEPTEMBER 2011 | DOI: 10.1038/NNANO.2011.105
nature nanotechnology

Thermodynamically stable RNA three-way junction for constructing multifunctional nanoparticles for delivery of therapeutics

Dan Shu[1†], Yi Shu[1†], Farzin Haque[1†], Sherine Abdelmawla[2] and Peixuan Guo[1*]

RNA nanoparticles have applications in the treatment of cancers and viral infection; however, the instability of RNA nanoparticles has hindered their development for therapeutic applications. The lack of covalent linkage or crosslinking in nanoparticles causes dissociation *in vivo*. Here we show that the packaging RNA of bacteriophage phi29 DNA packaging motor can be assembled from 3–6 pieces of RNA oligomers without the use of metal salts. Each RNA oligomer contains a functional module that can be a receptor-binding ligand, aptamer, short interfering RNA or ribozyme. When mixed together, they self-assemble into thermodynamically stable tri-star nanoparticles with a three-way junction core. These nanoparticles are resistant to 8 M urea denaturation, are stable in serum and remain intact at extremely low concentrations. The modules remain functional *in vitro* and *in vivo*, suggesting that the three-way junction core can be used as a platform for building a variety of multifunctional nanoparticles. We studied 25 different three-way junction motifs in biological RNA and found only one other motif that shares characteristics similar to the three-way junction of phi29 pRNA.

Living organisms produce a variety of highly ordered structures made up of DNA, RNA and proteins to perform diverse functions. DNA has been widely used as a biomaterial[1]. Even though RNA has many of the attributes of DNA that make it useful as a biomaterial, such as ease of manipulation, it has received less attention[2–4]. RNA also permits non-canonical base pairing and offers catalytic functions similar to some proteins[2]. Typically, RNA molecules contain a large variety of single-stranded stem–loops for inter- or intramolecular interactions[5]. These loops serve as mounting dovetails, which eliminates the need for external linking dowels during fabrication and assembly[3,6]. Since the discovery of siRNA[7], nanoparticles of siRNA[8–10], ribozymes[11–13], riboswitches[14,15] and microRNAs[16–18] have been explored for the treatment of cancers and viral infections.

One of the problems in the field of RNA nanotechnology is that RNA nanoparticles are relatively unstable; the lack of covalent binding or crosslinking in the particles causes dissociation at ultra-low concentrations in animal and human circulation systems after systemic injection. This has hindered the efficiency of delivery and therapeutic applications of RNA nanoparticles[2]. Although not absolutely necessary for RNA helix formation, tens of millimoles of magnesium are required for optimum folding of nanoparticles such as phi29 pRNA[19,20]. Because the concentration of magnesium under physiological conditions is generally less than 1 mM, misfolding and dissociation of nanostructures that use RNA as a scaffold can occur at these low concentrations.

The DNA packaging motor of bacteriophage phi29 is geared by a pRNA ring[21], which contains two functional domains[22,23]. The central domain of a pRNA subunit contains two interlocking loops, denoted as right- and left-handed loops, which can be engineered to form dimers, trimers or hexamers[3,20,24,25]. Because the two domains fold separately, replacing the helical domain with an siRNA does not affect the structure, folding or intermolecular interactions of the pRNA[8,26,27]. Such a pRNA/siRNA chimera has been shown to be useful for gene therapy[8–11]. The two domains are connected by a three-way junction (3WJ) region (Fig. 1c,d), and this unique structure has motivated its use in RNA nanotechnology. Here we show that the 3WJ region of pRNA can be assembled from three pieces of small RNA oligomers with high affinity. The resulting complex is stable and resistant to denaturation in the presence of 8 M urea. Incubation of three RNA oligomers, each carrying an siRNA, receptor-binding aptamer or ribozyme, resulted in trivalent RNA nanoparticles that are suitable as therapeutic agents. Of the 25 3WJ motifs obtained from different biological systems, we found the 3WJ-pRNA to be most stable.

Properties of 3WJ-pRNA

The 3WJ domain of phi29 pRNA was constructed using three pieces of RNA oligos denoted as a_{3WJ}, b_{3WJ} and c_{3WJ} (Fig. 1d). Two of the oligos, a_{3WJ} and c_{3WJ}, were resistant to staining by ethidium bromide (Fig. 2a) and weakly stained by SYBR Green II; c_{3WJ} remained unstainable (Fig. 2a). Ethidium bromide is an intercalating agent that stains double-stranded (ds) RNA and dsDNA or short-stranded (ss) RNA containing secondary structures or base stacking. SYBR Green II stains most ss- and ds-RNA or DNA. The absence of, or weak, staining indicates novel structural properties.

The mixing of the three oligos, a_{3WJ}, b_{3WJ} and c_{3WJ}, at a 1:1:1 molar ratio at room temperature in distilled water resulted in efficient formation of the 3WJ domain. Melting experiments suggest that the three components of the 3WJ-pRNA core (T_m of 58 °C) had a much higher affinity to interact favourably in comparison with any of the two components (Fig. 2b). The 3WJ domain remained stable in distilled water without dissociating at room temperature for weeks. If one of the oligos was omitted (Fig. 2a, lanes 4–6), dimers were observed, as seen by the faster migration rates compared with the 3WJ domain (Fig. 2a, lane 7). Generally, dsDNA and dsRNA are denatured and dissociate in the presence of 5 M (ref. 28) or 7 M urea (ref. 29). In the presence of 8 M urea, the 3WJ domain remained stable without dissociation (Fig. 2d), thereby demonstrating its robust nature.

[1]Nanobiomedical Center, University of Cincinnati, Cincinnati, Ohio 45267, USA, [2]Kylin Therapeutics, West Lafayette, Indiana 47906, USA; †These authors contributed equally to this work. *e-mail: guopn@ucmail.uc.edu

© 2011 Macmillan Publishers Limited. All rights reserved.

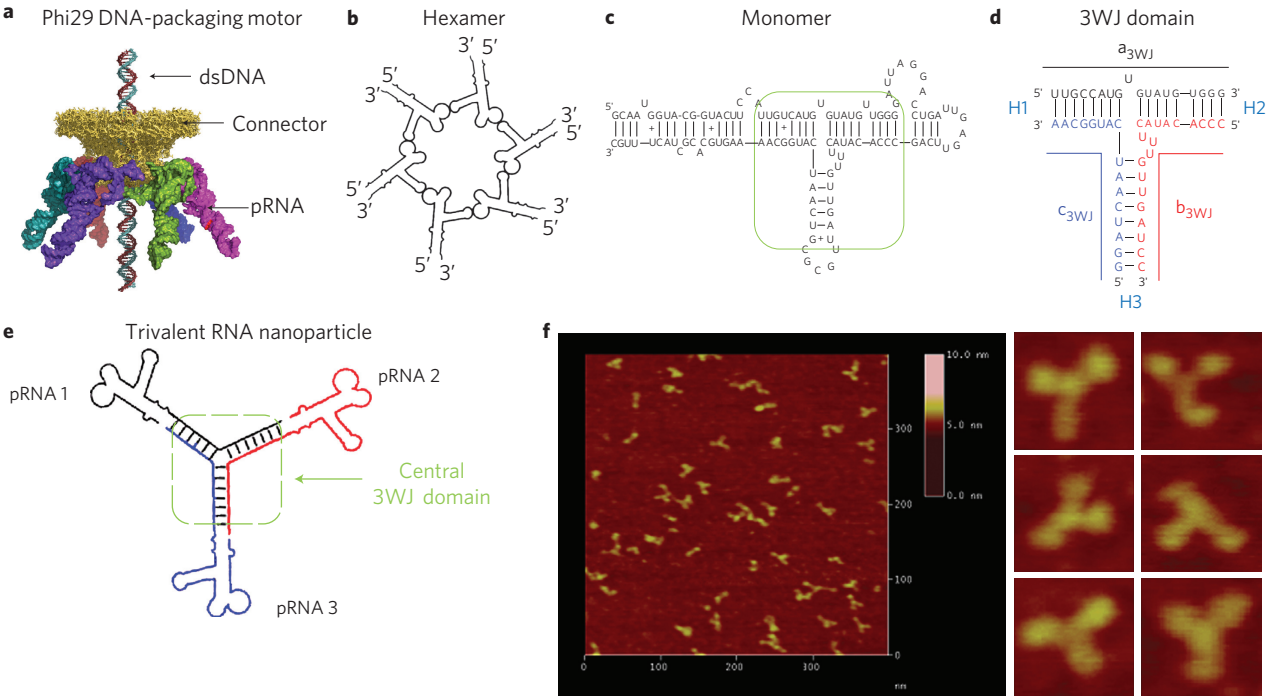

Figure 1 | Sequence and secondary structure of phi29 DNA-packaging RNA. a, Illustration of the phi29 packaging motor geared by six pRNAs (cyan, purple, green, pink, blue and orange structures). **b**, Schematic showing a pRNA hexamer assembled through hand-in-hand interactions of six pRNA monomers. **c**, Sequence of pRNA monomer Ab′ (ref. 3). Green box: central 3WJ domain. In pRNA Ab′, A and b′ represent right- and left-hand loops, respectively. **d**, 3WJ domain composed of three RNA oligomers in black, red and blue. Helical segments are represented as H1, H2, H3. **e**,**f**, A trivalent RNA nanoparticle consisting of three pRNA molecules bound at the 3WJ-pRNA core sequence (black, red and blue) (**e**) and its accompanying AFM images (**f**). Ab′ indicates non-complementary loops[35].

The lengths of helices H1, H2 and H3 were 8, 9 and 8 base pairs, respectively. RNA complexes with the deletion of two base pairs in H1 and H3 (Figs 1d and 2d) seem to have no effect on complex formation (Fig. 2d, lanes 8, 9). However, deletion of two base pairs at H2 (Figs 1d and 2d) did not affect complex formation, but made the 3WJ domain unstable in the presence of 8 M urea (Fig. 2d, lanes 7, 10). These results demonstrate that although six base pairs are sufficient in two of the stem regions, eight bases are necessary for H2 to keep the junction domain stable under strongly denaturing conditions.

To further evaluate the chemical and thermodynamic properties of 3WJ-pRNA, the same sequences were used to construct a DNA 3WJ domain. In native gel, when the three DNA oligos are mixed in a 1:1:1 molar ratio, the 3WJ-DNA assembled (Fig. 2e). However, the DNA 3WJ complex dissociated in the presence of 8 M urea (Fig. 2e, bottom). DNA–RNA hybrid 3WJ domains exhibited increasing stability as more RNA strands were incorporated. In essence, by controlling the ratio of DNA to RNA in the 3WJ domain region, the stability can be tuned accordingly.

To assess the stability of 3WJ-pRNA, we conducted competition experiments in the presence of urea and at different temperatures as a function of time. For a candidate therapeutic RNA nanoparticle, it is necessary to evaluate whether it would dissociate at a physiological temperature of 37 °C. A fixed concentration of the Cy3-labelled 3WJ-pRNA core was incubated with unlabelled b_{3WJ} at 25, 37 and 55 °C. At 25 °C, there is no exchange of labelled and unlabelled b_{3WJ} (Fig. 3a). At a physiological temperature of 37 °C, only a very small amount of exchange is observed in the presence of a 1,000-fold higher concentration of labelled b_{3WJ} (Fig. 3a). At 55 °C (close to the T_m of 3WJ-pRNA), there is approximately half-and-half exchange at a 10-fold excess concentration and near-complete exchange at a 1,000-fold higher concentration of labelled b_{3WJ} (Fig. 3a). These results are consistent with the T_m measurements.

A fixed concentration of the Cy3-labelled 3WJ-pRNA core was incubated with unlabelled b_{3WJ} at room temperature in the presence of 0–6 M urea. At equimolar concentrations (Cy3-$[ab^*c]_{3WJ}$:unlabelled $b_{3WJ} = 1:1$), there was little or no exchange under all the urea conditions investigated (Fig. 3b). At a fivefold higher concentration (Cy3-$[ab^*c]_{3WJ}$:unlabelled $b_{3WJ} = 1:5$), there was little or no exchange under 2 and 4 M urea conditions, and ~20% exchange at 6 M urea (Fig. 3b). Hence, 6 M urea 'destabilizes' the 3WJ-pRNA complex to only an insignificant extent.

Properties of 3WJ-pRNA with therapeutic modules

It has previously been demonstrated that the extension of phi29 pRNA at the 3′-end does not affect the folding of the pRNA global structure[26,27]. Sequences of each of the three RNA oligos, a_{3WJ}, b_{3WJ} and c_{3WJ}, were placed at the 3′-end of the pRNA monomer Ab′. Mixing the three resulting pRNA chimeras containing a_{3WJ}, b_{3WJ} and c_{3WJ} sequences, respectively, at equimolar concentrations led to the assembly of 3WJ branched nanoparticles harbouring one pRNA at each branch. Atomic force microscopy (AFM) images strongly confirmed the formation of larger RNA complexes with three branches (Fig. 1e,f), which were consistent with gel shift assays. This nanoparticle can also be co-transcribed and assembled in one step during transcription with high yield (data not shown).

When RNA nanoparticles are delivered systemically to the body, these particles can exist at low concentrations because of dilution by circulating blood. Only those RNA particles that are intact at low concentrations can be considered as therapeutic agents for systemic delivery. To determine whether the larger structure with three branches harbouring multi-module functionalities is dissociated at low concentration, this [^{32}P]-labelled complex was serially diluted to extremely low concentrations: the concentration for dissociation was below the detection limit of [^{32}P]-labelling technology. Even at

© 2011 Macmillan Publishers Limited. All rights reserved.

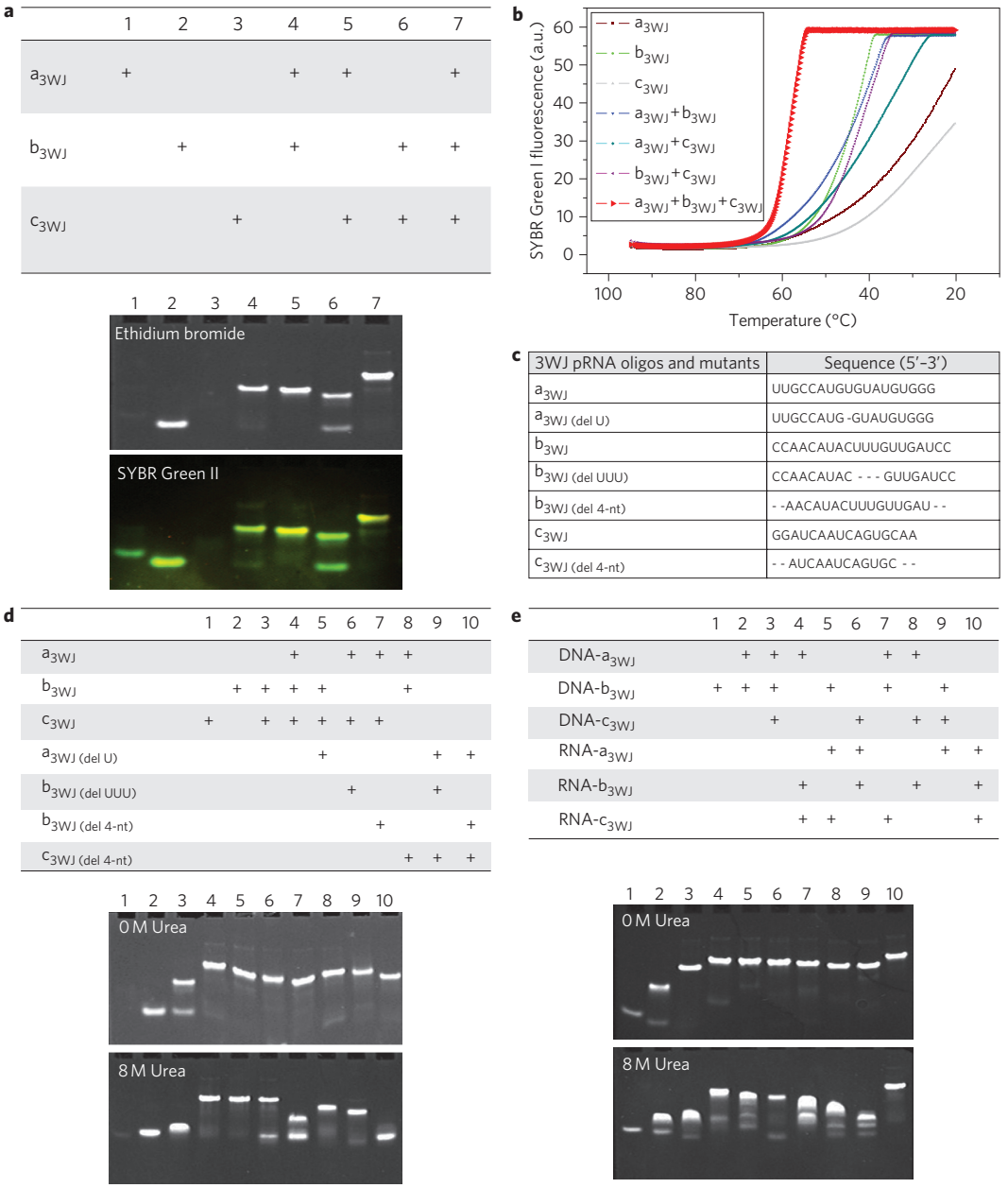

Figure 2 | Assembly and stability studies of 3WJ-pRNA. In the tables, '+' indicates the presence of the strand in samples of the corresponding lanes. **a**, 15% native PAGE showing the assembly of the 3WJ core, stained by ethidium bromide (upper) and SYBR Green II (lower). **b**, T_m melting curves for the assembly of the 3WJ core. Melting curves for the individual strands (brown, green, silver), the two-strand combinations (blue, cyan, pink) and the three-strand combination (red) are shown. **c**, Oligo sequences of 3WJ-pRNA cores and mutants. 'del U', deletion of U bulge; 'del UUU', deletion of UUU bulge; 'del 4-nt', deletion of two nucleotides at the 3′ and 5′ ends, respectively. **d**, Length requirements for the assembly of 3WJ cores and stability assays by urea denaturation. **e**, Comparison of DNA and RNA 3WJ core in native and urea gel.

160 pM in TMS buffer, which was the lowest concentration tested, the dissociation of nanoparticles was undetectable (Fig. 3c).

Multi-module RNA nanoparticles were constructed using this 3WJ-pRNA domain as a scaffold (Fig. 4a). Each branch of the 3WJ carried one RNA module with defined functionality, such as a cell-receptor-binding ligand, aptamer, siRNA or ribozyme. The presence of modules or therapeutic moieties did not interfere with the formation of the 3WJ domain, as demonstrated by AFM imaging (Fig. 4c). Furthermore, the chemically modified (2′-F U/C) 3WJ-pRNA therapeutic complex was resistant to degradation in cell culture medium with 10% serum even after 36 h of incubation, whereas the unmodified RNA degraded within 10 min (Supplementary Fig. S3).

In vitro and *in vivo* assessments of multi-module 3WJ-pRNA

Making fusion complexes of DNA or RNA is not hard to achieve, but ensuring the appropriate folding of individual modules within the complex after fusion is a difficult task. To test whether the incorporated RNA moieties retain their original folding and functionality after being fused and incorporated, hepatitis B virus (HBV)-cleaving ribozyme[11] and MG (malachite green dye, triphenylmethane)-binding aptamer[30] were used as model systems for structure and function verification. Free MG is not fluorescent by itself, but emits fluorescent light after binding to the aptamer.

HBV ribozyme was able to cleave its RNA substrate after being incorporated into the nanoparticles (Fig. 4d), and fused MG-binding aptamer retained its capacity to bind MG, as demonstrated

© 2011 Macmillan Publishers Limited. All rights reserved.

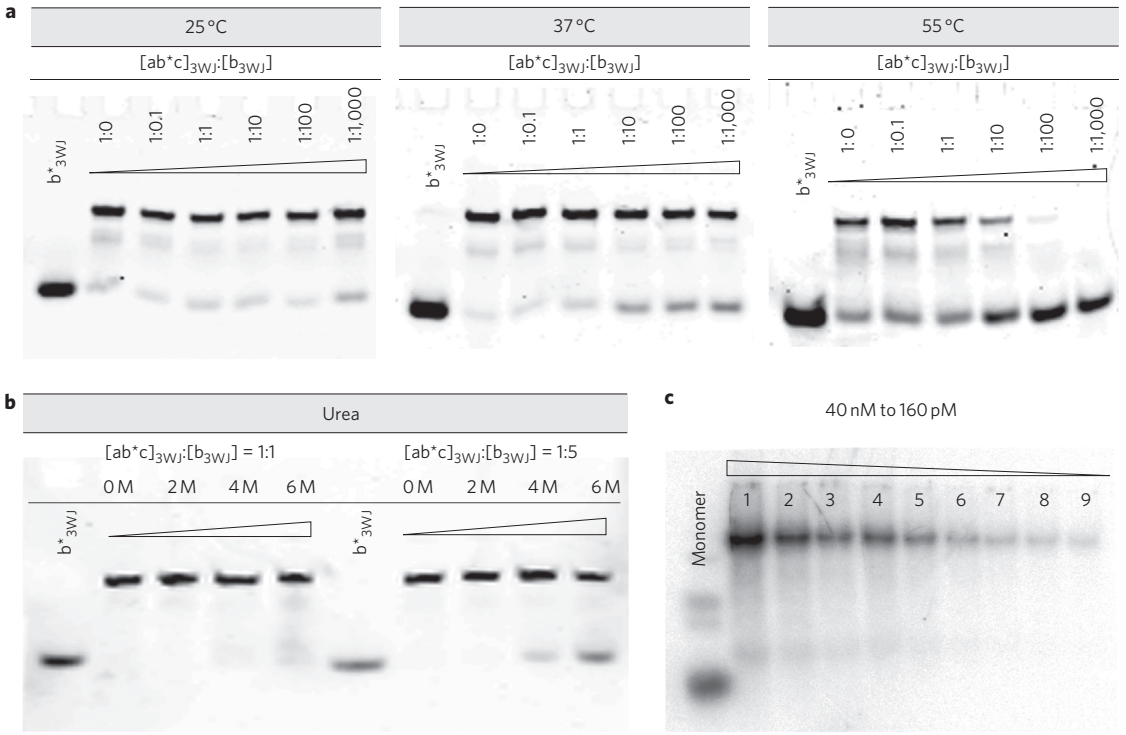

Figure 3 | Competition and dissociation assays of 3WJ-pRNA. a, Temperature effects on the stability of the 3WJ-pRNA core, denoted as $[ab^*c]_{3WJ}$, evaluated by 16% native gel. A fixed concentration of Cy3-labelled $[ab^*c]_{3WJ}$ was incubated with varying concentrations of unlabelled b_{3WJ} at 25, 37 and 55 °C. **b**, Urea denaturing effects on the stability of $[ab^*c]_{3WJ}$ evaluated by 16% native gel. A fixed concentration of labelled $[ab^*c]_{3WJ}$ was incubated with unlabelled b_{3WJ} at ratios of 1:1 and 1:5 in the presence of 0–6 M urea at 25 °C. **c**, Dissociation assay for the [^{32}P]-3WJ-pRNA complex harbouring three monomeric pRNAs by twofold serial dilution (lanes 1–9). The monomer unit is shown on the left.

by its fluorescence emission (Fig. 4f). The activity results are comparable to optimized positive controls and therefore confirm that individual RNA modules fused into the nanoparticles retained their original folding after incorporation into the RNA nanoparticles.

Several cancer cell lines, especially of epithelial origin, overexpress the folate receptor on the surface by a factor of 1,000. Folate has been used extensively as a cancer cell delivery agent through folate-receptor-mediated endocytosis[31]. The 2′-F U/C-modified fluorescent 3WJ-pRNA nanoparticles with folate conjugated into one of their branches were tested for cell binding efficiency. One fragment of the 3WJ-pRNA core was labelled with folic acid for targeted delivery[10], the second fragment was labelled with Cy3 and the third fragment was fused to siRNA that could silence the gene of the anti-apoptotic factor, Survivin[32]. Negative controls included RNA nanoparticles that contained folate but a scrambled siRNA sequence, and a 3WJ-pRNA core with active siRNA but without folate. Flow cytometry data showed that the folate-3WJ-pRNA nanoparticles bound to the cell with almost 100% binding efficiency (Fig. 5a, Supplementary Fig. S4). Confocal imaging indicated strong binding of the RNA nanoparticles and efficient entry into targeted cells, as demonstrated by the excellent co-localization and overlap of fluorescent 3WJ-pRNA nanoparticles (red) and the cytoplasm (green) (Fig. 5b).

Two 3WJ-RNA nanoparticles were constructed for assaying the gene silencing effect. Particle [3WJ-pRNA-siSur-Rz-FA] harbours folate and Survivin siRNA, and particle [3WJ-pRNA-siScram-Rz-FA] harbours folate and Survivin siRNA scramble as control. After 48 h transfection, both quantitative reverse transcription-polymerase chain reaction (qRT–PCR) and western blot assays confirmed a reduced Survivin gene expression level for 3WJ-pRNA-siSur-Rz-FA compared with the scramble control on both messenger RNA and protein levels. The silencing potency is comparable to the positive Survivin siRNA-only control, although the reduction of both the RNA complexes was modest (Fig. 5c).

Two key factors that may affect the pharmacokinetic profile are metabolic stability and renal filtration. It has been reported that regular siRNA molecules have extremely poor pharmacokinetic properties, because they have a short half-life ($T_{1/2}$) and fast kidney clearance as a result of metabolic instability and small size (<10 nm)[33]. The pharmacokinetic profile of AlexaFluor647-2′-F-pRNA nanoparticles that use the 3WJ domain as a scaffold was studied in mice on systemic administration of a single intravenous injection through the tail vein, followed by blood collection[49]. The concentration of the fluorescent nanoparticle in serum was determined. The half-life ($t_{1/2}$) of the pRNA nanoparticles was determined to be 6.5–12.6 h, compared with control 2′F-modified siRNA, which could not be detected beyond 5 min post-injection, which is close to the $t_{1/2}$ of 35 min reported in the literature[34].

To confirm that RNA nanoparticles were not dissociated into individual subunits *in vivo*, these nanoparticles were constructed by a bipartite approach[49,51] with one subunit carrying the folate to serve as a ligand for binding to the cancer cells, and the other subunit carrying a fluorescent dye. The nanoparticles were systemically injected into mice through the tail vein[49]. Whole-body imaging showed that fluorescence was located specifically at the xenographic cancer expressing the folate receptor and was not detected in other organs of the body (Fig. 5e), and indicated that the particles did not dissociate *in vivo* after systemic delivery.

Comparing 3WJ-pRNA with other biological 3WJ motifs

There are many 3WJ motifs in biological RNA, some of which are stabilized by extensive tertiary interactions and non-canonical base pairings and base stacking[35–40]. To assess whether the

© 2011 Macmillan Publishers Limited. All rights reserved.

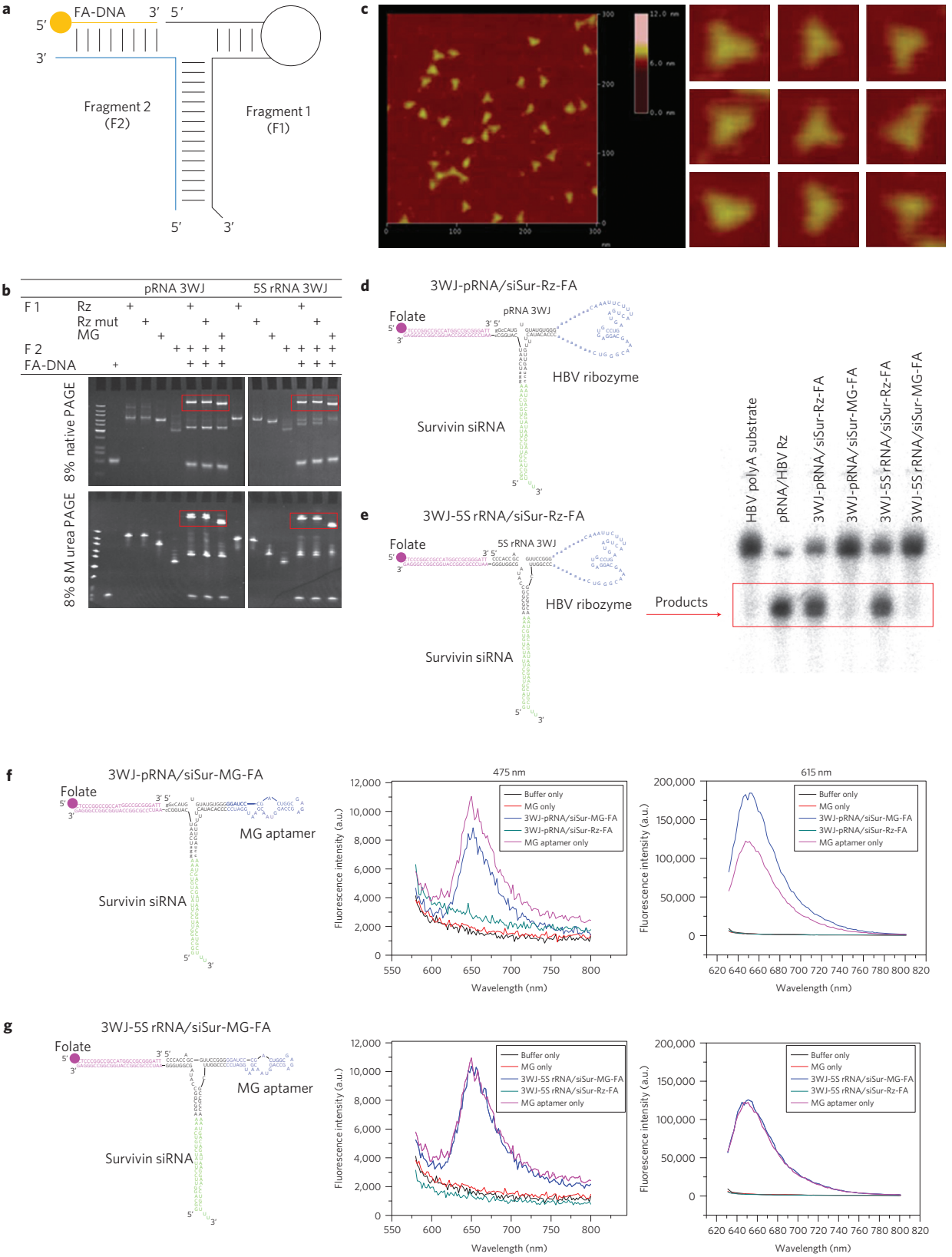

Figure 4 | Construction of multi-module RNA nanoparticles harbouring siRNA, ribozyme and aptamer. a–c, Assembly of RNA nanoparticles with functionalities using 3WJ-pRNA and 3WJ-5S rRNA as scaffolds. **a–c**, Illustration (**a**), 8% native (upper) and denaturing (lower) PAGE gel (**b**) and AFM images (**c**) of 3WJ-pRNA-siSur-Rz-FA nanoparticles. **d**,**e**, Assessing the catalytic activity of the HBV ribozyme incorporated into the 3WJ-pRNA (**d**) and 3WJ-5S rRNA (**e**) cores, evaluated in 10% 8 M urea PAGE. The cleaved RNA product is boxed. Positive control: pRNA/HBV-Rz; negative control: 3WJ-RNA/siSur-MG-FA. **f**,**g**, Functional assay of the MG aptamer incorporated in RNA nanoparticles using the 3WJ-pRNA (**f**) and 3WJ-5S rRNA (**g**) cores. MG fluorescence was measured using excitation wavelengths of 475 and 615 nm.

© 2011 Macmillan Publishers Limited. All rights reserved.

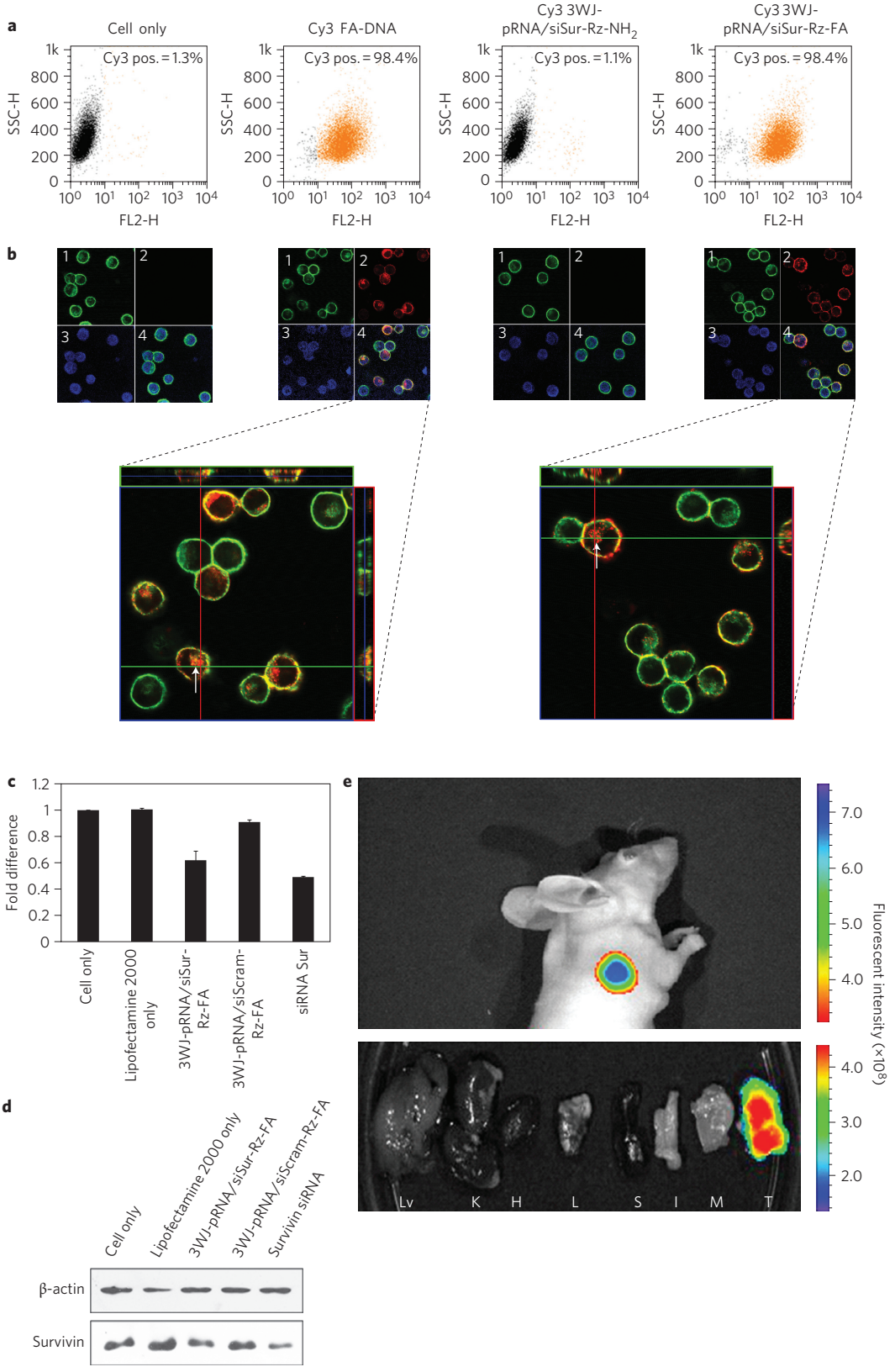

Figure 5 | *In vitro* and *in vivo* binding and entry of 3WJ-pRNA nanoparticles into targeted cells. a, Flow cytometry revealed the binding and specific entry of fluorescent-[3WJ-pRNA-siSur-Rz-FA] nanoparticles into folate-receptor-positive (FA^+) cells. Positive and negative controls were Cy3-FA-DNA and Cy3-[3WJ-pRNA-siSur-Rz-NH_2] (without FA), respectively. **b**, Confocal images showed targeting of FA^+-KB cells by co-localization (overlap, 4) of cytoplasm (green, 1) and RNA nanoparticles (red, 2) (magnified, bottom panel). Blue–nuclei, 3. **c**,**d**, Target gene knock-down effects shown by (**c**) qRT-PCR with GADPH as endogenous control and by (**d**) western blot assay with β-actin as endogenous control. **e**, 3WJ-pRNA nanoparticles target FA^+ tumour xenografts on systemic administration in nude mice. Upper panel: whole body; lower panel: organ imaging (Lv, liver; K, kidney; H, heart; L, lung; S, spleen; I, intestine; M, muscle; T, tumour).

© 2011 Macmillan Publishers Limited. All rights reserved.

Table 1 | Comparison of biophysical properties of various 3WJ cores.

Family	Name	Sequence 5′–3′	Assembly of 3WJ-RNA core		Assembly of 3WJ-pRNA with three pRNA monomers		T_m (°C)
			Native gel	8 M urea denaturing gel	Native gel	8 M urea denaturing gel	TMS buffer
A 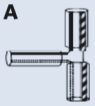	16s H34-H35-H38	a, GGG GAC GAC GUC b, CGA GCG CAA CCC CC c, GUC GUC AGC UCG	Weak	No	Yes	No	45.3±6.7
	23s H75-H76-H79	a, GAG GAC ACC GA b, GGC UCU CAC UC c, UCG CUG AGC C	No	No	No	No	33.3±0.6
B 	23s H83-H84-H85	a, AGC AAA AGA U b, CCC GGC GAA GAG UG c, AUC UCA GCC GGG	No	No	No	No	53.7±0.6
C 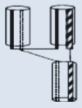	5s rRNA	a, CCC GGU UCG CCG CCA b, CCC ACC AGC GUU CCG GG c, AGG CGG CCA UAG CGG UGG G	Very strong	Very strong	Yes	Yes	54.3±3.1
	G-Riboswitch (Type I)	a, GGA CAU AUA AUC GCG UG b, AUG UCC GAC UAU GUC C c, CAC GCA AGU UUC UAC CGG GCA	Medium	No	Yes	No	46.0±3.5
	TPP Riboswitch (Type II)	a, GCG ACU CGG GGU GCC CUU C b, GAA GGC UGA GAA AUA CCC GUA UCA CCU GAU CUG G c, CCA GCG UAG GGA AGU CGC	Strong	No	Yes	No	52.0±4.4
	M-box Riboswitch (Type II)	a, GAC GCC AAU GGG UCA ACA GAA AUC AUC G b, AGG UGA UUU UUA AUG CAG CU c, ACG CUG CUG CCC AAA AAU GUC	Strong	No	Yes	No	45.3±5.5
	Hammerhead ribozyme	a, CUG UCA CCG GAU b, GGA CGA AAC AG c, UUC CGG UCU GAU GAG UCC	No	No	No	No	49.7±1.5
	Alu SRP	a, GGG CCG GGC GCG GU b, UCG GGA GGC UC c, GGC GCG CGC CUG UAG UCC CAG C	No	No	No	No	45.3±4.6
Unknown	HCV	a, UCA UGG UGU UCC GGA AAG CGC b, GUG AUG AGC CGA UCG UCA GA c, UCU GGU GAU ACC GAG A	No	No	No	No	49.7±1.5
	pRNA	a, UUG CCA UGU GUA UGU GGG b, CCC ACA UAC UUU GUU GAU CC c, GGA UCA AUC AUG GCA A	Very strong	Very strong	Yes	Yes	58.0±0.5

Note: The sequences of the 3WJ cores were obtained from refs 39, 41–43. Families A, B and C are based on the Lescoute and Westhof classification[39]. The other 14 3WJ cores that were not practical for thorough investigations are listed in Supplementary Table S2.

properties of the 3WJ-pRNA core are unique, we thoroughly investigated the assembly and stability of 25 3WJ motifs (Table 1 and Supplementary Table S2) reported in the literature[35,39,41–43]. Of the 25 motifs, 14 were impractical to study using core sequences; for example, some were too short (less than 10 nt for one of their fragments) for chemical synthesis. Using synthesized RNA fragments with the exact sequences as reported, with appropriate controls, the other 11 motifs were thoroughly investigated. Only 6 of the 11 structures were able to assemble into a 3WJ complex, based on gel shift assays (Table 1 and Fig. 6). However, in the presence of 8 M urea, only the 3WJ-pRNA core and the 3WJ-5S ribosomal RNA core were stable. The Alu SRP appears to have assembled; however, with appropriate controls (Supplementary Fig. S1), it was found that the band was from the strong folding of one individual RNA fragment (a_{3WJ}) by itself, rather than the assembly of a 3WJ.

Moreover, 25 different RNA nanoparticles were constructed using each of the central 3WJ motifs as the scaffold to test their potential for constructing RNA nanoparticles harbouring three functionalities with extended sequences (Supplementary Fig. S2). Here, we used individual phi29 pRNA subunits as modules[3,23–26]. The sequences for each of the three oligos comprising individual 3WJ were placed at the 3′-end of the 117-nt pRNA, thereby serving as sticky ends. On co-transcription (of three pRNA strands harbouring the sticky end sequences of 3WJ, respectively), 10 of the 25 constructs were able to assemble into a 3WJ complex through the sticky ends representing the three fragments of 3WJ, as demonstrated by gel shift assays (Supplementary Fig. S2). However, only two of the constructs (3WJ-pRNA and 3WJ-5S rRNA) were resistant to 8 M urea denaturation, which is consistent with RNA oligo assembly data (Fig. 6). These results suggest that only 3WJ-5S rRNA is comparable to 3WJ-pRNA, and therefore 3WJ-5S rRNA can also serve as a platform to organize RNA modules bearing different functionalities.

To test whether the functionalities incorporated in the nanoparticles with the 3WJ core display catalytic or binding function, HBV ribozyme and MG aptamer were incorporated into RNA nanocomplexes. Both HBV ribozyme (Fig. 4d,e) and MG aptamer were

© 2011 Macmillan Publishers Limited. All rights reserved.

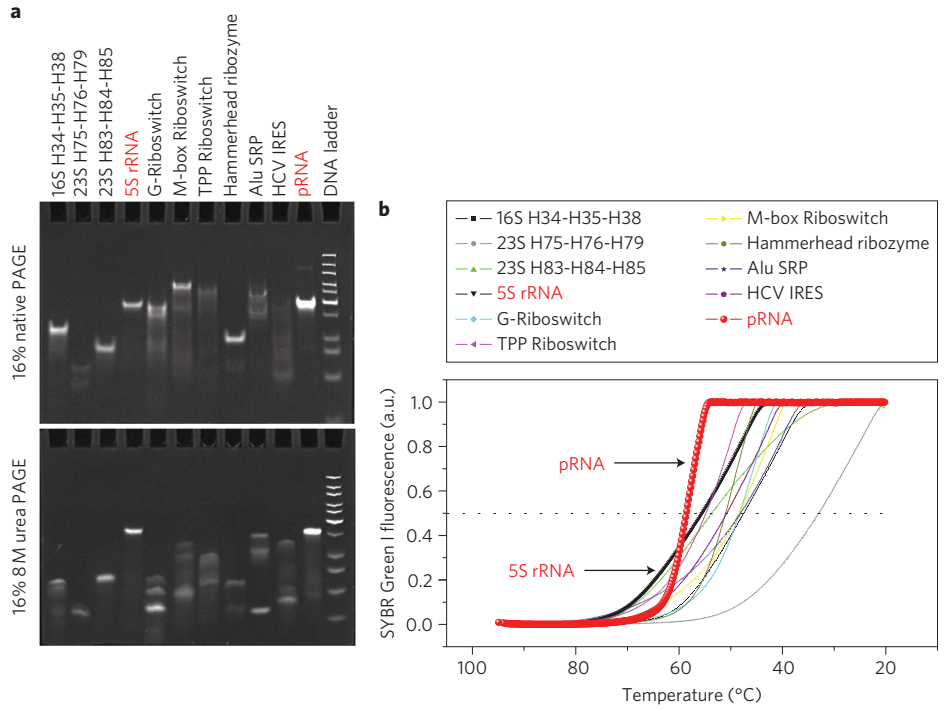

Figure 6 | Comparison of different 3WJ-RNA cores. a, Assembly and stability of 11 3WJ-RNA core motifs assayed in 16% native (upper) and 16% 8 M urea (lower) PAGE gel. **b**, Melting curves for each of the 11 RNA 3WJ core motifs assembled from three oligos for each 3WJ motif under physiological buffer TMS. Refer to Table 1 for the respective T_m values.

functional after being incorporated into 3WJ-pRNA or 3WJ-5S rRNA, respectively (Fig. 4f,g), suggesting that 3WJ-5S rRNA is comparable to 3WJ-pRNA for constructing complexes harbouring different RNA functionalities for cell delivery.

One of the most important parameters for evaluating therapeutic RNA nanoparticles is their thermodynamic stability under physiological conditions *in vivo*. T_m studies on three oligos for each of the 11 3WJ motifs were conducted in physiological buffer containing 5 mM $MgCl_2$ and 100 mM NaCl at pH 7.6 (Fig. 6 and Table 1). Among the assembled 3WJ structures, pRNA showed the highest T_m (58 °C). The T_m closest to 3WJ-pRNA was that of 3WJ-5S rRNA (54.3 °C).

The affinity and efficiency of assembly were further investigated by both gel retardation assay and melting experiments (data shown only for 3WJ-pRNA (Fig. 2a,b), 3WJ-5S rRNA and 3WJ-Alu SRP cores) (Supplementary Fig. S1). 3WJ-pRNA displayed a very smooth high-slope temperature-dependent melting curve, and clean bands in the gel, clearly indicating the assembly of monomer, dimer and 3WJ with little or no residual RNA fragments (Fig. 2a,b). The results suggest that the three components of 3WJ-pRNA have a much higher affinity to interact favourably in comparison with any of the two components. Furthermore, the sharp melting transition indicates cooperative simultaneous folding of the three helical stems. In contrast, 3WJ-5S rRNA and all the other 3WJ motifs display temperature-dependent in the T_m curve with lower slopes (Fig. 6b). Titration of the three oligos of the 3WJ-5S rRNA system showed that mixing of only two of the three RNA fragments resulted in the formation of a urea-sensitive band with a migration rate even slower than that of the entire 3WJ complex (Supplementary Fig. S1). This suggests that the individual fragment or the two-fragment combination of 3WJ-5S rRNA might have undesired binding affinities that interfere with the final 3WJ assembly. Nevertheless, the affinity of the three-component interaction is sufficiently higher than that of the two-component interaction in the 3WJ-5S rRNA system to drive the assembly of the final 3WJ structure. For Alu SRP, the folding of individual strands significantly interferes with the formation of 3WJ, and hence the complex does not assemble (Supplementary Fig. S1).

Although systematic comparison of the assembly and stability of different 3WJs has not been reported, there are several limited studies on T_m measurements of individual 3WJ motifs[44–48]. Some studies explain the thermodynamic factors that govern the folding of 3WJ RNA motifs, such as hairpin ribozyme[45] and intact stem–loop messenger RNA[46]. Thermodynamic parameters of a variety of constructs (mutations and insertions) based on the structure and sequence of the 3WJ core of 5S-rRNA have been reported[44,47,48], but they have only used a two-strand system instead of the three-fragment approach, and hence the results are not directly comparable. Nevertheless, the results are consistent with our findings.

In conclusion, these results suggest that the phi29 3WJ domain has the potential to serve as a platform for the construction of RNA nanoparticles containing multiple functionalities for the delivery of therapeutics to specific cells for the treatment of cancer, viral infection and genetic diseases. We thoroughly evaluated 25 3WJ motifs in biological RNA and identified 3WJ-5S rRNA as the only 3WJ motif comparable to 3WJ-pRNA for constructing complexes harbouring different functionalities. Nevertheless, we found that 3WJ-pRNA is the most stable nanoparticle with the sharpest slope in the T_m curve (Fig. 6b).

Methods

Construction of multi-module RNA nanoparticles. Sequences for each of the RNA strands, a_{3WJ}, b_{3WJ} and c_{3WJ}, were added to the 3′-end of each 117-nt pRNA-Ab′ (Fig. 1e). pRNA-a_{3WJ}, pRNA-b_{3WJ} and pRNA-c_{3WJ} were then synthesized *in vitro* by transcription of the corresponding DNA template by T7 RNA polymerase. The 3WJ-pRNA harbouring three monomeric pRNAs was then self-assembled by mixing the three subunits in equal molar concentrations. Alternatively, the three individual templates can be co-transcribed and assembled in one step followed by purification in 8% native polyacrylamide gel electrophoresis (PAGE).

Sequences for siRNA, HBV ribozyme, MG-binding aptamer and folate-labelled RNA were rationally designed with sequences of the strands a_{3WJ}, b_{3WJ} and c_{3WJ}, respectively (Fig. 4, Supplementary Table S2). Multi-module 3WJ-pRNA-HBV

© 2011 Macmillan Publishers Limited. All rights reserved.

ribozyme-Survivin siRNA-folate (3WJ-pRNA-siSur-Rz-FA) or 3WJ-pRNA-MG aptamer-Survivin siRNA-folate (3WJ-pRNA-siSur-MG-FA) was assembled from four individual fragments, including a 26-nt folate-labelled RNA (Trilink) or folate-DNA strand (synthesized in-house), and a chemically synthesized 21-nt siRNA or scramble siRNA anti-sense strand (IDT). The 106-nt strand harbouring HBV ribozyme sequence, the 96-nt strand harbouring MG-binding aptamer and the 41-nt strand harbouring siRNA sense strand were transcribed from DNA template amplified by PCR (Supplementary Table S2). Fluorescent dyes were labelled on the 106-nt RNA strand by using the Label IT siRNA Tracker Intracellular Localization Kit, Cy3™ (Mirus Bio LLC). The four RNA strands were mixed after purification in TMS buffer at equal molar ratios, and then heated up to 80 °C for 5 min followed by slow cooling to 4 °C. The assembled nanoparticles were then purified from 8% native PAGE gel.

Competition assays and radiolabel chasing. Competition experiments were carried out in the presence of urea and at different temperatures as a function of time. The Cy3-labelled 3WJ-pRNA core $[ab^*c]_{3WJ}$ was constructed using three RNA oligos, a_{3WJ}, Cy3-b_{3WJ} and c_{3WJ}, mixed in a 1:1:1 molar ratio in diethylpyrocarbonate (DEPC)-treated water or TMS buffer.

Presence of urea: the concentration of labelled $[ab^*c]_{3WJ}$ was fixed; unlabelled b_{3WJ} was incubated with labelled $[ab^*c]_{3WJ}$ for 30 min at room temperature in the presence of variable concentrations of urea (0–6 M). The samples were then loaded onto 16% native gel. Two concentration ratios were evaluated: $[ab^*c]_{3WJ}$: unlabelled b_{3WJ} = 1:1 and 1:5.

Different temperatures: the concentration of labelled $[ab^*c]_{3WJ}$ was fixed, and varying concentration ratios of unlabelled b_{3WJ} (1:0–1:1,000) were incubated with labelled $[ab^*c]_{3WJ}$ for 30 min at 25, 37 and 55 °C and then loaded onto 16% native gel.

Dilution assay to test dissociation at extremely low concentrations: the stability of the 3WJ-pRNA complex harbouring three monomeric pRNAs was evaluated by radiolabel assays. The purified [^{32}P]-complexes were serially diluted from 40 to 160 pM in TMS buffer and then loaded onto 8% native PAGE gel.

Melting experiments for T_m. Melting experiments were conducted by monitoring the fluorescence of the 3WJ RNAs using the LightCycler 480 Real-Time PCR System (Roche). 1× SYBR Green I dye (Invitrogen) (emission 465–510 nm), which binds double-stranded nucleic acids but not single-stranded ones, was used for all the experiments. The respective RNA oligonucleotides (IDT) were mixed at room temperature in physiological TMS buffer. The 3WJ RNA samples were slowly cooled from 95 to 20 °C at a ramping rate of 0.11 °C s^{-1}. Data were analysed by LightCycler 480 Software using the first derivative of the melting profile. The T_m value represents the mean and standard deviation of three independent experiments.

HBV ribozyme activity assay. HBV ribozyme is an RNA enzyme that cleaves the genomic RNA of HBV genome[11]. HBV RNA substrate was radiolabelled by [α-^{32}P] UTP (PerkinElmer) and incubated with the 3WJ-pRNA or 3WJ-5S rRNA core harbouring HBV ribozyme at 37 °C for 60 min in a buffer containing 20 mM $MgCl_2$, 20 mM NaCl and 50 mM Tris-HCl (pH 7.5). The pRNA/HBV ribozyme served as a positive control[11], and 3WJ RNA harbouring MG aptamer was used as a negative control (Fig. 4). The samples were then loaded on 8 M urea/10% PAGE gel for autoradiography.

MG aptamer fluorescence assay. 3WJ-pRNA or 3WJ-5S rRNA trivalent RNA nanoparticles harbouring MG-binding aptamer[30] (100 nM) were mixed with MG (2 μM) in binding buffer containing 100 mM KCl, 5 mM $MgCl_2$ and 10 mM HEPES (pH 7.4) and incubated at room temperature for 30 min (Fig. 4f,g). Fluorescence was measured using a fluorospectrometer (Horiba Jobin Yvon), excited at 475 nm (540–800 nm scanning for emission) and 615 nm (625–800 nm scanning for emission).

Methods for synthesis and purification of pRNA; construction and purification of pRNA complexes; serum stability assays; flow cytometry analysis of folate-mediated cell binding[51]; confocal microscopy imaging[51]; assays for the silencing of genes in a cancer cell model; stability and systemic pharmacokinetic analysis in animals[49]; targeting of tumour xenograft by systemic injection in animals[49]; and AFM imaging[50] can be found in the Supplementary Information.

Received 1 April 2011; accepted 8 June 2011; published online 11 September 2011

References

1. Seeman, N. C. Nanomaterials based on DNA. *Annu. Rev. Biochem.* **79,** 65–87 (2010).
2. Guo, P. The emerging field of RNA nanotechnology. *Nature Nanotech.* **5,** 833–842 (2010).
3. Guo, P. *et al.* Inter-RNA interaction of phage phi29 pRNA to form a hexameric complex for viral DNA transportation. *Mol. Cell.* **2,** 149–155 (1998).
4. Shukla, G. C. *et al.* A boost for the emerging field of RNA nanotechnology. *ACS Nano* **5,** 3405–3418 (2011).
5. Cruz, J. A. & Westhof, E. The dynamic landscapes of RNA architecture. *Cell* **136,** 604–609 (2009).
6. Jaeger, L., Verzemnieks, E. J. & Geary, C. The UA_handle: a versatile submotif in stable RNA architectures. *Nucleic Acids Res.* **37,** 215–230 (2009).
7. Fire, A. *et al.* Potent and specific genetic interference by double-stranded RNA in *Caenorhabditis elegans*. *Nature* **391,** 806–811 (1998).
8. Khaled, A., Guo, S., Li, F. & Guo, P. Controllable self-assembly of nanoparticles for specific delivery of multiple therapeutic molecules to cancer cells using RNA nanotechnology. *Nano Lett.* **5,** 1797–1808 (2005).
9. Guo, S., Tschammer, N., Mohammed, S. & Guo, P. Specific delivery of therapeutic RNAs to cancer cells via the dimerization mechanism of phi29 motor pRNA. *Hum. Gene Ther.* **16,** 1097–1109 (2005).
10. Guo, S., Huang, F. & Guo, P. Construction of folate-conjugated pRNA of bacteriophage phi29 DNA packaging motor for delivery of chimeric siRNA to nasopharyngeal carcinoma cells. *Gene Ther.* **13,** 814–820 (2006).
11. Hoeprich, S. *et al.* Bacterial virus phi29 pRNA as a hammerhead ribozyme escort to destroy hepatitis B virus. *Gene Ther.* **10,** 1258–1267 (2003).
12. Sarver, N. A. *et al.* Ribozymes as potential anti-HIV-1 therapeutic agents. *Science* **247,** 1222–1225 (1990).
13. Liu, H. *et al.* Phi29 pRNA vector for efficient escort of hammerhead ribozyme targeting survivin in multiple cancer cells. *Cancer Biol. Ther.* **6,** 697–704 (2007).
14. Winkler, W. C. *et al.* Control of gene expression by a natural metabolite-responsive ribozyme. *Nature* **428,** 281–286 (2004).
15. Mulhbacher, J., St-Pierre, P. & Lafontaine, D. A. Therapeutic applications of ribozymes and riboswitches. *Curr. Opin. Pharmacol.* **10,** 551–556 (2010).
16. Chen, Y. *et al.* Nanoparticles modified with tumor-targeting scFv deliver siRNA and miRNA for cancer therapy. *Mol. Ther.* **18,** 1650–1656 (2010).
17. Pegtel, D. M. *et al.* Functional delivery of viral miRNAs via exosomes. *Proc. Natl Acad. Sci. USA* **107,** 6328–6333 (2010).
18. Ye, X., Liu, Z., Hemida, M. & Yang, D. Mutation tolerance and targeted delivery of anti-coxsackievirus artificial MicroRNAs using folate conjugated bacteriophage Phi29 pRNA. *PLoS ONE* **6,** e21215 (2011).
19. Chen, C. & Guo, P. Magnesium-induced conformational change of packaging RNA for procapsid recognition and binding during phage phi29 DNA encapsidation. *J. Virol.* **71,** 495–500 (1997).
20. Chen, C., Sheng, S., Shao, Z. & Guo, P. A dimer as a building block in assembling RNA: a hexamer that gears bacterial virus phi29 DNA-translocating machinery. *J. Biol. Chem.* **275,** 17510–17516 (2000).
21. Guo, P., Erickson, S. & Anderson, D. A small viral RNA is required for *in vitro* packaging of bacteriophage phi29 DNA. *Science* **236,** 690–694 (1987).
22. Reid, R. J. D., Bodley, J. W. & Anderson, D. Characterization of the prohead-pRNA interaction of bacteriophage phi29. *J. Biol. Chem.* **269,** 5157–5162 (1994).
23. Zhang, C. L., Lee, C.-S. & Guo, P. The proximate 5′ and 3′ ends of the 120-base viral RNA (pRNA) are crucial for the packaging of bacteriophage ϕ29 DNA. *Virology* **201,** 77–85 (1994).
24. Shu, D., Zhang, H., Jin, J. & Guo, P. Counting of six pRNAs of phi29 DNA-packaging motor with customized single molecule dual-view system. *EMBO J.* **26,** 527–537 (2007).
25. Xiao, F., Moll, D., Guo, S. & Guo, P. Binding of pRNA to the N-terminal 14 amino acids of connector protein of bacterial phage phi29. *Nucleic Acids Res.* **33,** 2640–2649 (2005).
26. Shu, D. *et al.* Bottom-up assembly of RNA arrays and superstructures as potential parts in nanotechnology. *Nano Lett.* **4,** 1717–1723 (2004).
27. Zhang, C. L., Trottier, M. & Guo, P. X. Circularly permuted viral pRNA active and specific in the packaging of bacteriophage Phi29 DNA. *Virology* **207,** 442–451 (1995).
28. Carlson, R. D., Olins, A. L. & Olins, D. E. Urea denaturation of chromatin periodic structure. *Biochemistry* **14,** 3122–3125 (1975).
29. Pagratis, N. C. Rapid preparation of single stranded DNA from PCR products by streptavidin induced electrophoretic mobility shift. *Nucleic Acids Res.* **24,** 3645–3646 (1996).
30. Baugh, C., Grate, D. & Wilson, C. 2.8 Å crystal structure of the malachite green aptamer. *J. Mol. Biol.* **301,** 117–128 (2000).
31. Lu, Y. & Low, P. S. Folate-mediated delivery of macromolecular anticancer therapeutic agents. *Adv. Drug Deliv. Rev.* **54,** 675–693 (2002).
32. Ambrosini, G., Adida, C. & Altieri, D. C. A novel anti-apoptosis gene, survivin, expressed in cancer and lymphoma. *Nature Med.* **3,** 917–921 (1997).
33. Soutschek, J. *et al.* Therapeutic silencing of an endogenous gene by systemic administration of modified siRNAs. *Nature* **432,** 173–178 (2004).
34. Behlke, M. A. Progress towards *in vivo* use of siRNAs. *Mol. Ther.* **13,** 644–670 (2006).
35. Chen, C., Zhang, C. & Guo, P. Sequence requirement for hand-in-hand interaction in formation of pRNA dimers and hexamers to gear phi29 DNA translocation motor. *RNA* **5,** 805–818 (1999).
36. de la, P. M., Dufour, D. & Gallego, J. Three-way RNA junctions with remote tertiary contacts: a recurrent and highly versatile fold. *RNA.* **15,** 1949–1964 (2009).
37. Lilley, D. M. Structures of helical junctions in nucleic acids. *Q. Rev. Biophys.* **33,** 109–159 (2000).
38. Afonin, K. A. *et al. In vitro* assembly of cubic RNA-based scaffolds designed in silico. *Nature Nanotech.* **5,** 676–682 (2010).

© 2011 Macmillan Publishers Limited. All rights reserved.

39. Lescoute, A. & Westhof, E. Topology of three-way junctions in folded RNAs. *RNA* **12,** 83–93 (2006).
40. Leontis, N. B. & Westhof, E. Analysis of RNA motifs. *Curr. Opin. Struct. Biol.* **13,** 300–308 (2003).
41. Honda, M., Beard, M. R., Ping, L. H. & Lemon, S. M. A phylogenetically conserved stem-loop structure at the 5′ border of the internal ribosome entry site of hepatitis C virus is required for cap-independent viral translation. *J. Virol.* **73,** 1165–1174 (1999).
42. Wakeman, C. A., Ramesh, A. & Winkler, W. C. Multiple metal-binding cores are required for metalloregulation by M-box riboswitch RNAs. *J. Mol. Biol.* **392,** 723–735 (2009).
43. Kulshina, N., Edwards, T. E. & Ferre-D'Amare, A. R. Thermodynamic analysis of ligand binding and ligand binding-induced tertiary structure formation by the thiamine pyrophosphate riboswitch. *RNA* **16,** 186–196 (2010).
44. Diamond, J. M., Turner, D. H. & Mathews, D. H. Thermodynamics of three-way multibranch loops in RNA. *Biochemistry* **40,** 6971–6981 (2001).
45. Klostermeier, D. & Millar, D. P. Helical junctions as determinants for RNA folding: origin of tertiary structure stability of the hairpin ribozyme. *Biochemistry* **39,** 12970–12978 (2000).
46. Rettberg, C. C. *et al.* A three-way junction and constituent stem-loops as the stimulator for programmed -1 frameshifting in bacterial insertion sequence IS911. *J. Mol. Biol.* **286,** 1365–1378 (1999).
47. Liu, B., Diamond, J. M., Mathews, D. H. & Turner, D. H. Fluorescence competition and optical melting measurements of RNA three-way multibranch loops provide a revised model for thermodynamic parameters. *Biochemistry* **50,** 640–653 (2011).
48. Mathews, D. H. & Turner, D. H. Experimentally derived nearest-neighbor parameters for the stability of RNA three- and four-way multibranch loops. *Biochemistry* **41,** 869–880 (2002).
49. Abdelmawla, S. *et al.* Pharmacological characterization of chemically synthesized monomeric pRNA nanoparticles for systemic delivery. *Mol. Ther.* **19,** 1312–1322 (2011).
50. Lyubchenko, Y. L. & Shlyakhtenko, L. S. AFM for analysis of structure and dynamics of DNA and protein-DNA complexes. *Methods* **47,** 206–213 (2009).
51. Shu, Y. *et al.* Assembly of therapeutic pRNA-siRNA nanoparticles using bipartite approach. *Mol. Ther.* **19,** 1304–1311 (2011).

Acknowledgements

This research was mainly supported by the National Institutes of Health (NIH; grants EB003730, GM059944 and CA151648 to P.G.). P.G. is also a co-founder of Kylin Therapeutics Inc. The authors thank L. Shlyakhtenko and Y. Lyubchenko for AFM images via the Nanoimaging Core Facility supported by the NIH SIG Program and the UNMC Program of ENRI, as well as N. Abdeltawab and Z. Zhu from M. Kotb's laboratory at the University of Cincinnati for help with qRT–PCR assays.

Author contributions

P.G. conceived, designed and led the project. D.S., Y.S. and F.H. designed and conducted the *in vitro* experiments. S.A. performed animal imaging experiments. P.G., D.S., Y.S. and F.H. analysed the data and co-wrote the manuscript.

Additional information

The authors declare competing financial interests: details accompany the full-text HTML version of the paper at www.nature.com/naturenanotechnology. Supplementary information accompanies this paper at www.nature.com/naturenanotechnology. Reprints and permission information is available online at http://www.nature.com/reprints. Correspondence and requests for materials should be addressed to P.G.

© 2011 Macmillan Publishers Limited. All rights reserved.